Effect of the surrounding fluid on the compaction of granular materials by tapping: Slow dynamics made slower?

Shi Han Ng and Hans-Georg Matuttis

Department of Mechanical Engineering and Intelligent Systems, Graduate School of Informatics and Engineering, The University of Electro-Communications, Chofugaoka 1-5-1, Chofu, Tokyo 182-8585, Japan

Abstract. We investigate compaction due to tapping in two-dimensional granular columns computationally with the discrete element method (DEM) in two dimensions. We compare the compaction in dry granulates with the compaction of the system immersed in a viscous fluid. We use polygons as particle shapes, so that the resulting pore-space can be triangulated for a finite element method (FEM) for an incompressible fluid. We investigate the competition between a slowing-down of the dynamics due to the viscous forces of the fluid and the improved transmission of the tapping pulses through the fluid in the pore space. For the system immersed in water, the propagation of the shocks due to the tapping of the floor is faster than in the corresponding dry system. The center of mass of a nearly square system drops faster for the dry case than for immersed particles. For a system twice as high and half as wide, for the same vibration, for the dry system, the center of mass rises, while for the immersed particles there is hardly any change.

Keywords: Nonlinear acoustical and dynamical systems, granular flow classical mechanics of discrete systems, complex fluids
PACS: 43.25.Ts, 45.70.-n, 45.70.Mg, 47.57.Gc

1. INTRODUCTION

The relaxation of granular materials is a paradigm of "slow" dynamics: The resulting compaction is logarithmically slow [1, 2, 3]. For realistic granular materials (i.e. those with solid friction), the questions of what is an equilibrium state is not easily settled: While conventionally, the equilibrium state is considered to be the state which is obtained "long enough", it is not clear what "long enough" means in the present of static (Coulomb) friction, which acts effectively as a constraint of motion, so that no relaxation takes place at all in this static equilibrium. If a granular material which is initially in a static state is excited, depending on the excitation (shaking, vibration, pneumatic driving . . .), the resulting density may be higher or lower than that of the static state before the excitation. We want to investigate computationally the compaction under tapping (acceleration of boundaries) of granular columns so that between the excitations, the system can return again to a static state for both the case of dry material, as well as for particles fully immersed under a viscous Newtonian fluid.

1.1. Previous research on compaction in tapped granular material

Since the investigation by Knight et al. [1, 2, 3] compaction in granular matter has been established to be logarithmically slow. Experimentally, tapping has been investigated predominantly for round glass beads [4, 5, 6, 7], but more recently also more irregularly shaped [8] and even needle-shaped particles [9] particles have been used in the investigation. Because of the logarithmically slow dynamics, in computational investigations rule-based models [9, 10, 11] have been preferred to cover large time scales, but recently, also discrete element simulations have been used [12]. Due to the slowness of the dynamics, analytical investigations have been undertaken [13] despite the complexity of the system. One point which should not be forgotten about granular compaction with tapping is that the long-time limit is not necessarily the densest packing available for a given kind of material: For some materials, higher packings can be obtained by first evacuating the vessel with the granular filling and then letting the air stream in [14].

1.2. Research outline

We limit ourselves to the computational investigation of two-dimensional granular systems with and without liquid. We are interested in the change in the short time dynamics when a very viscous fluid is introduced into the pore space. While conventionally granular materials are simulated in the discrete element method with round shapes, we use a polygonal simulation to take into account the fact that in realistic granular particles, reordering by rotation in the bulk is hardly possible.

We compare the relaxation behavior under tapping for the dry granular material with that for particles immersed in a relatively viscous fluid ($\mu_f = 1[\mathrm{Pa}\cdot\mathrm{s}]$, thousand times

Effect of the surrounding fluid on the compaction of granular materials by tapping: Slow dynamics made slower?
AIP Conf. Proc. 1518, pp. 372-378; doi:http://dx.doi.org/10.1063/1.4794599 (7 pages)
4TH INTERNATIONAL SYMPOSIUM ON SLOW DYNAMICS IN COMPLEX SYSTEMS: Keep Going Tohoku
Date: 2–7 December 2012
Location: Sendai, Japan
Shi Han Ng and Hans-Georg Matuttis

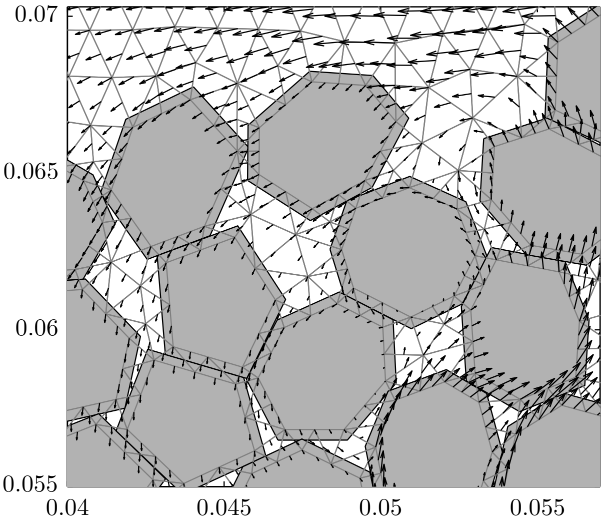

FIGURE 1. Microscopic simulation of fluid flow around particles in a shadow.

the viscosity of water) to see how the character of the relaxation changes due to the presence of fluid. The simulation is "microscopic", i.e. the boundaries of the particles are the boundaries for the fluid (see Figure 1), the fluid can move only in this pore space, in contrast to "macroscopic" simulations of fluid with particles where the fluid can go "through" the particles [15]. Because there are hardly any codes for microscopic simulations, and the numerical solution of the flow field is rather more costly than the DEM-simulation, we limit ourselves to the initial time of the compaction. Nevertheless, we can establish long-term limits by reducing or altogether switching off the static friction, see sec. 6.1.

While the viscous fluid can be imagined to increase the damping in the relaxation process, on the other hand it can be expected to improve the transmission of the excitation through the granular column, when particle do not push only neighboring particles, but also buoyancy of the surrounding fluid to transmit the tapping impulse: The particle-particle interstices themselves are relatively "weak links", so that the sound velocity on the surface of a polygonal granular assembly is of the order of 10% of the sound velocity of the corresponding continuum material [16] $c = \sqrt{Y/\rho}$ given by its Young modulus Y and density ρ. The question is which element will gain the upper hand: The additional damping, the lubrication by the fluid or the enhanced transmission.

2. DISCRETE ELEMENT METHOD

In the discrete element method (DEM), the granular aggregate is modeled by individual grains. In our method,

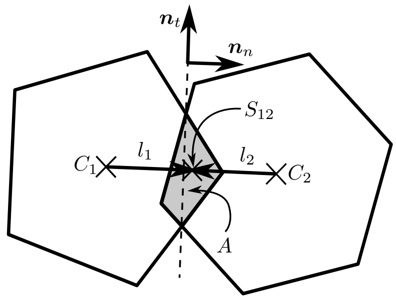

FIGURE 2. Sketch of the geometry of a particle-particle contact for the polygonal simulation.

polygonal particles are represented as rigid polygons (no macroscopic deformation), while the force between neighboring particles is proportional to their area overlap ("hard particle, soft contact") [17]. When two particles are in contact (see Figure 2), we compute the elastic contact force between them proportional to the overlap area A of the undeformed particles as

$$F_{c,\perp} = Y \cdot \frac{A}{l}, \tag{1}$$

where Y is the Young's modulus in two dimensions (i.e. with units N/m). The characteristic length l is defined as $l_1 \cdot l_2/(l_1 + l_2)$, with l_1 and l_2 as the lengths from the center of mass of the particles to the force point ("hard particle, soft contact"). The characteristic length l serves to adapt the sound velocity in a space filling packing to the sound velocity of the continuum material [16]. We define the damping term in normal direction as

$$F_{d,\perp} = \gamma \sqrt{Y m_{\mathrm{red}}} \frac{1}{l} \frac{\mathrm{d}A}{\mathrm{d}t}, \tag{2}$$

where γ is the damping constant and $m_{\mathrm{red}} = m_1 m_2/(m_1 + m_2)$ is the reduced mass of the contacting particles. Additionally, an if-condition prevents that the damping force in Eq. (2) for separation can overcompensate the elastic repulsive force from Eq. (1) to eliminate unphysical spurious attractive forces [16] which would act as a source of noise. To model static Coulomb friction, the tangential force is defined incrementally [18] as

$$F_{d,\|}(t) = F_{d,\|}(t - \Delta t) + Y_t \cdot v_t \cdot \Delta t + \sqrt{m_{\mathrm{eff},\|} \cdot Y_t} v_t \tag{3}$$

if $F_{d,\|}(t) \leq \mu \cdot F_\perp$, else it is $\mu \cdot F_\perp$ where $F_\perp = F_{d,\perp} + F_{c,\perp}$ is the tangential force. In Eq. 3, $m_{\mathrm{eff},\|}$ is the reduced tangential mass which can be written as

$$m_{\mathrm{eff},\|} = \frac{1}{1/m_1 + 1/m_2 + l_1^2/I_1 + l_2^2/I_2}, \tag{4}$$

where I_1 and I_2 are the momenta of inertia of the particles. The tangential Young's modulus is defined as $Y_t =$

$Y \cdot 2/7$. If not indicated otherwise, we use a friction coefficient of $\mu = 0.3$ (both for the static and dynamic friction, both between particles as well as between particles and walls) for the dry system as well as for the system of immersed particles, to make clear up in the differences in the dynamics which comes from the introduction of the fluid. For many particles materials, the friction coefficient of the fluid-immersed particles would probably be lower. We neglect inter-particle cohesion, though it can be modeled quite easily in our DEM-approach [19]. These equations of motion for the particle simulation are solved using the second order backward difference formula (BDF2, Gear predictor-corrector of 2nd-order [20]).

The grains in the two-dimensional system can be imagined as "rods" in three dimensions. Our units are chosen so that the particles are taken to be rods of one meter length. The density of the granular particles is $5000[\mathrm{kg/m^2}]$ (respective to a depth of $1[\mathrm{m}]$), while the bulk density (including the pore space) varies between $4195[\mathrm{kg/m^3}]$ and $4280[\mathrm{kg/m^3}]$, e.g. the porosity of around 0.39 (including particle shadows), 0.16 (without the particle shadows). The Young's modulus is $10^6[\mathrm{N/m}]$ (again, respective to a depth of $1[\mathrm{m}]$), the damping constant is 1.5. The Young's modulus may look small compared to the ones for three dimensional materials like stone, which are of the order of several hundred gigapascal. Nevertheless, in our simulation, smooth sides are in contact, while in real materials, it would be surface asperities which would lead to the contacts, which are much easier to deform.

3. FINITE ELEMENT METHOD

In granular materials without additional compression, the sound velocity is considerably lower than for the respective continuum (below 10% of the continuum sound velocity in two dimensions, below 1% in three) [16]. As the sound propagation through the granular matrix is relatively slow, we work with an incompressible fluid. We choose a formulation where the pressure are computed as Lagrange-parameters in each timestep. The resulting differential algebraic equation is solved most efficiently via an implicit integrator, so we have resorted to the formulation of the Navier-Stokes equation from Gresho et al. [21] as

$$\begin{pmatrix} \frac{3}{2\Delta t}M + K + N(u_{n+1}) & -C \\ C^T & 0 \end{pmatrix} \begin{pmatrix} u_{n+1} \\ P_{n+1} \end{pmatrix} = \begin{pmatrix} M\left[\frac{2}{\Delta t}u_n - \frac{1}{2\Delta t}u_{n-1}\right] + f_{n+1} \\ 0 \end{pmatrix}, \qquad (5)$$

as second order backward difference formula (BDF2), as the particle trajectories. with the mass matrix M,the viscous matrix K, the non-linear terms N, the external forces f, the flow velocities u and the pressures P. C is the matrix for the incompressibility constraint, $\nabla \cdot \vec{u} = 0$. We solve Eq. (5) via Newton-Raphson iteration [22]. The inversion of the Jacobian in our MATLAB-implementation, we use the backslash-solver, which calls UMFPACK-routines. Krylov-solvers turned out to be inefficient, as the velocities and the pressures in Eq. (5) have different scaling.

The packing of polygons creates a void space which can be tessellated exactly with triangles. The discretization of choice for such irregular domains is via the Finite Element method (FEM) for irregular meshes. The discretization is via P_2P_1 triangular elements (Taylor-Hood elements), with pressures on the corners of the triangular elements [22]. Accordingly, the pressures are also defined of the boundary of the fluid domain, which is important for the computation of the interaction between particles and fluids. The triangulation of the pore space is obtained as constraint Delaunay triangulation (i.e. the constraint is that the mesh may not extend into the particle) with additional relaxation ob avoid degenerated triangles [23]. We work with the density of water ($1000[\mathrm{kg/m^3}]$) and a viscosity of $1[\mathrm{Pa \cdot s}]$.

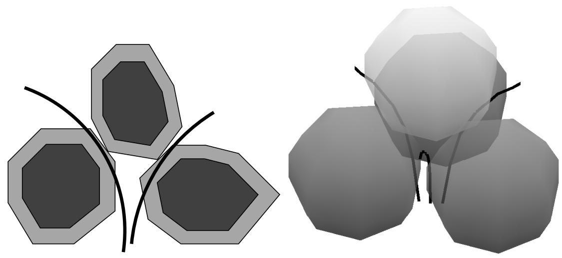

FIGURE 3. Left: Fluid space (white), shadow by which the particles interact (light gray) and core (dark gray) which forms the boundary of the fluid flow. Right: Three-dimensional arrangement of grains which leads to flow between the particles along the fat lines which is supposed to be mimicked by the shadow on the left.

4. COUPLING OF DEM AND FEM

To model the pore-space in such a way that blocking of pore regions is avoided as in the realistic three dimensional dynamics, the particles consist of a core, whose boundary is a boundary of the fluid, and a "shadow" which is used to for the computation of the interaction between the granular particles. Inside this shadow, the fluid flow is computed as for the empty space to obtain a pore space is connected, so that no sub-volumes are closed of, as would be the case for three dimensional particles, see Figure 3. The size ratio between the the whole particle and the core is about 1 : 0.72.

Boundary conditions for the flow on the surface of the particle core are no-slip conditions: Interaction between the flow and the particles takes place via the forces of the particles on the surface, namely, the form drag

$$F_x^P = -\int_\Gamma n_x P \mathrm{d}l \quad , \quad F_y^P = -\int_\Gamma n_y P \mathrm{d}l, \qquad (6)$$

due to the pressure computed according to equation (5) as Lagrange parameters, and friction drag (proportional to the gradient of the flow tangential to the particle surfaces)

$$F_x^V = \mu_\mathrm{f} \int_\Gamma 2n_x \mathrm{d}u\mathrm{d}x + n_y (\mathrm{d}u\mathrm{d}y + \mathrm{d}v\mathrm{d}x)\, \mathrm{d}l, \qquad (7)$$

$$F_y^V = \mu_\mathrm{f} \int_\Gamma 2n_y \mathrm{d}v\mathrm{d}y + n_x (\mathrm{d}u\mathrm{d}y + \mathrm{d}v\mathrm{d}x)\, \mathrm{d}l, \qquad (8)$$

where Γ is the boundary of the particle's interface and μ_f is the dynamic viscosity of the fluid.

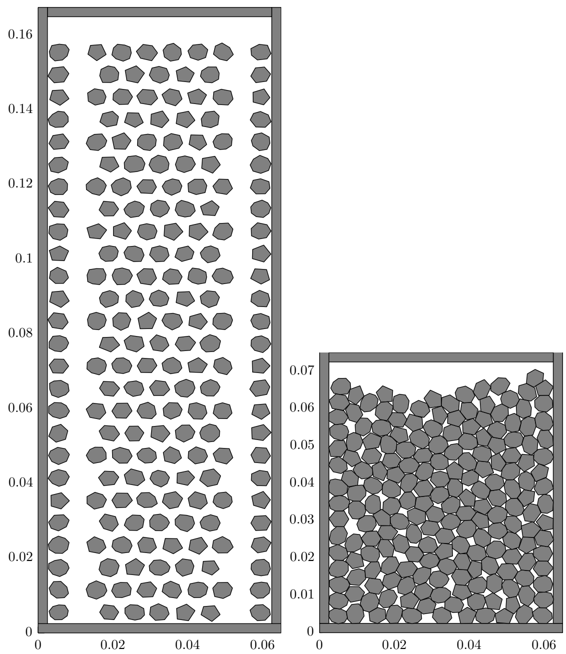

FIGURE 4. Initialization of the "wide" system with 195 (left) and system with the particles settled down which is used as initial configuration.

5. SYSTEM SETUP

In the following, we treat two different geometries one nearly square ("wide") with 195 particles, one which is about four times as high as it is wider ("narrow system") with 190 particles.

5.1. Preparation of the initial system

The particle shape is constructed by inscribing regular polygons into ellipses (Semi-major axis of 1.2, semi-minor axis of 1) and randomize the shapes and sizes by adding random numbers of $\pm 10\%$ of the radius for the corners. Only convex particles are used. The corner numbers of the particles range between 5 and 9. We construct the initial configuration of the granular packing by dropping the particles in the dry DEM-simulation from initial positions with the center on a regular grid (Figure 4, left) and wait until the particles have settled down and the vibrations in the agglomerate are damped out (Figure 4, right). In the initial grid (Figure 4, left), a stripe of particles is left near the left and right boundary to allow the development of stronger disorder than what is possible if the positions are occupied regularly. We start with the same initial configuration (position, orientation, friction value) for the dry and the immersed system. To offset the effect of buoyancy, we simulated the dry system with density $5000[\mathrm{kg/m^3}]$, and the immersed system with density $6000[\mathrm{kg/m^3}]$, inside a fluid with density $1000[\mathrm{kg/m^3}]$.

6. TAPPING

For modeling the tapping, i.e. conferring an impulse to the particle system via the boundaries, we have several possibilities. The tapping can be implemented as a displacement of the boundaries, or a specification of a velocity of the boundary (without displacing the boundary at all) or as a combination of both. Because sudden displacements of a neighboring particle can lead to very large shocks, we opted for keeping the wall position constant and change only the (dummy) velocity on the walls surface. Next we have to decide which boundaries we want to manipulate: We can tap either only a part of the boundaries, i.e. the floor, or all the boundaries. In physical systems, tapping the floor of a cylindrical vessel will lead to a propagation of the shock also along the cylinders walls: To transmit momentum only through tapping of the bottom, it would have to be unconnected to the cylinder's walls. We decided to investigate both possibilities: Tapping of the bottom was used so that the upward propagation of the shock wave through the system could be measured (sec. 7.1), and the differences in shock propagation with and without fluid could be identified. Tapping of the whole boundary (sec. 7.2, 7.3) was used in the hope of enforce a more physical macroscopic rearrangements of the granular matrix.

The duration of the pulse is $0.001[\mathrm{s}]$, the time between the beginning of one pulse and the beginning of the next is $0.4[\mathrm{s}]$, see Figure 7. Together with the magnitude of the pulse, we rather quantify the response, i.e. we give

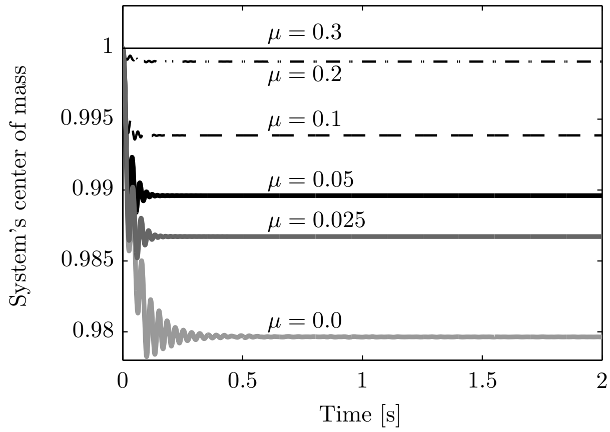

FIGURE 5. Position of the center of mass for reducing the coefficient of friction μ.

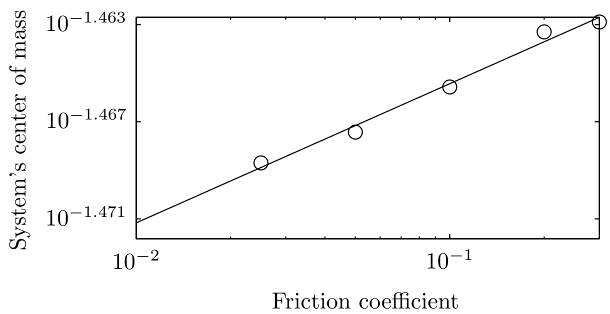

FIGURE 6. "Final" potential energy of the wide system with different coefficients of friction μ in double logarithmic plots ($\circ$) and the fitting (solid line).

time evolution of the acceleration for a particle in the lowest layer. The ratio between average acceleration by the pulse and gravitational acceleration ($9.81[\mathrm{m/s^2}]$) was $\bar{\Gamma} = 17.3$, with a maximal value of $\Gamma_{\max} = 64.4$. While for the system in fluid, the ratio was $\bar{\Gamma} = 18.8$, with a maximal value of $\Gamma_{\max} = 32.7$.

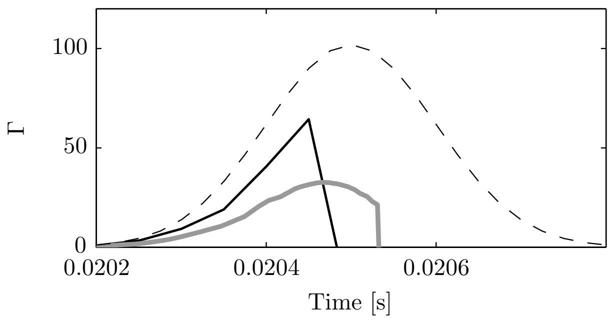

FIGURE 7. Time evolution of the acceleration of a particle in the lowest layer of the dry simulation (black) and wet simulation (gray) as well as intensity of the original pulse (dashed line).

6.1. Evolution of the center of mass

We monitor the evolution of the center of mass over time as the parameter of the relaxation, rather than the density: As our system does not have many particles, the upper layer is relatively large, compared to the total system, and it is difficult to define the upper boundary of the system and therefore the density with respect to the upper layer. To avoid this ambiguity, and to be able to compare systems of different dimensions, we use the position of the center of mass scaled to 1 as the parameter.

Vibration of particles in sliding contact is known to lead to continuous slipping [24]. Therefore, we computed the relaxation of the dry system without fluid from the initial configuration when the friction coefficient is reduced towards zero, see Figure 5. The packing density increases (i.e. the center of mass is lowered) monotonously with lowered coefficient of friction. This should give a plausible long-term limit, as vibration or tapping leads to a momentary reduction of the contact, which allows slipping, as would a reduction of the friction coefficient. The packing for vanishing static friction is a limiting case for the packing density, though it may not be the actual limit, depending on the choice of the tapping pulse. The dependence of the center of mass is not logarithmic, but a power law (see Figure 6).

Additionally, one can see in Figure 5 that the vibration is damped faster if the friction coefficient is high. The effect of the normal damping in Eq. (2) is weaker than that of the Coulomb friction from Eq. (3).

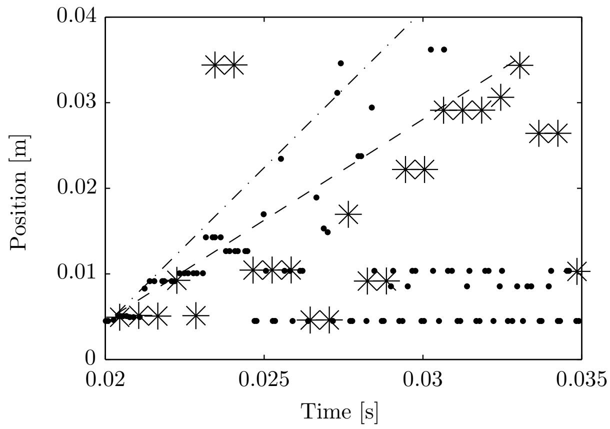

FIGURE 8. Shock propagation through the system for the dry ($*$) and the immersed system ($\bullet$) for tapping of the bottom. The symbols denote the position of the particle with the maximal dislocation over the time of the vibration pulse (see Figure 7) for a given timestep. The wavefronts for the immersed system are indicated by the dash-dotted line, for the dry system by the dashed line to guide the eye.

7. RESULTS

7.1. Wide system, tapping of the bottom only

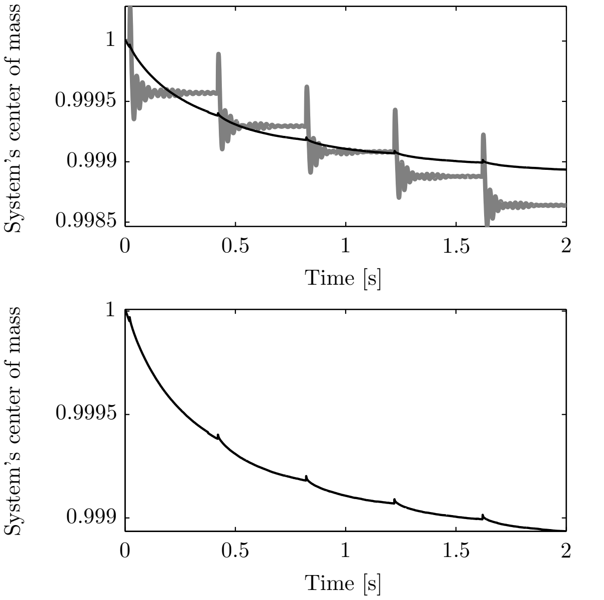

FIGURE 9. Compaction of the wide system with tapping only the bottom for the dry (above, solid line in gray) and the immersed particles (above, solid line in black), as well as latter zoomed (below).

The shock wave induced by the tapping on the bottom is shown in Figure 8 via the position of the particle which experiences the stronges dislocation from one timestep to the next. Several particles at different height are only weakly connected in the granular matrix, so that their rattling inside a "cage" of particles which are stiffly connected in the matrix is hardly damped, especially for the system without fluid (strings of the same symbols at different height in Figure 8). The sound wave in the dry system propagates with a speed of 2.36[m/s], while in the immersed system, it propagates with 3.68[m/s]. The sound velocity of the continuum material would be 14.1[m/s] for the dry and 12.9[m/s] for the immersed material. The corresponding fronts of the sound waves are indicated in Figure 8 with dash-dotted (immersed system) and dashed (dry system) lines. The surrounding fluid seems to be able to speed up the propagation speed of the shock wave though the continuum sound velocity of the material for the particles is lower. The sound wave is so much higher than in [16], because due to the compaction on the bottom, the particle contacts are pre-stressed and therefore much stiffer than on the surface.

The compaction results for the wide system which is tapped on the bottom (0.06[m] width, 0.07[m] height, 195 particles) are shown in Figure 9. The vibrations are damped more strongly in the fluid than in the dry system. While initially, the centers of mass of both the dry and the immersed particle system started out at 1, the center of mass of the dry system falls faster, as can be seen by the increasing distance between the gray and the black curve in Figure 9.

7.2. Wide system, boundary tapping of the whole wall

The compaction results for the wide system (same dimensions as the previous system) for which the tapping is felt at the whole wall are shown in Figure 10. The initial amplitude for the system with tapping of the whole boundary is about 11 times as large than for tapping with the same intensity on the bottom only. The compaction is consistent with the previous section. As in the case of tapping of the bottom, when the whole boundary is tapped, the center of mass in the dry system falls faster: With both systems' initially centers of mass of at 1, the gray curve for the dry system separates from the black curve for the immersed system in Figure 10.

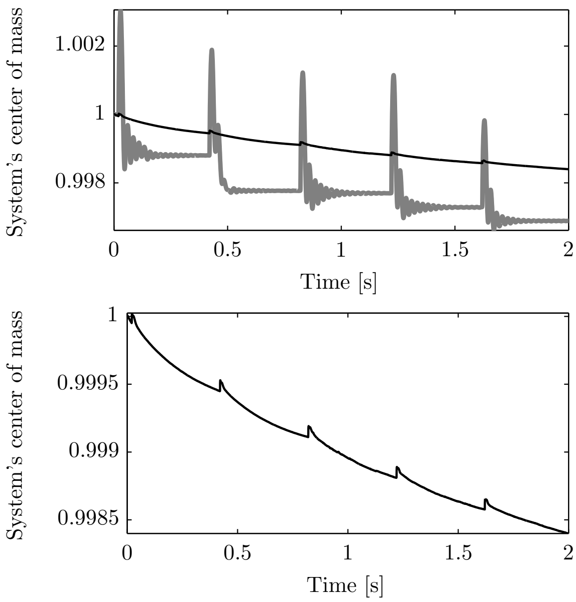

FIGURE 10. Compaction of the wide system for the dry (above, solid line in gray) and the immersed particles (above, solid line in black), as well as latter zoomed (below).

7.3. Narrow system, boundary tapping of the whole wall

The compaction results for the narrow system (0.03[m] width, 0.135[m] height, 190 particles) for which the tapping is felt at the whole wall are shown in Figure 11.

Surprisingly, the center of mass rises for the dry system while the system with fluid is hardly affected. The damping (decay of the oscillations) is much stronger than for the square system, which shows the influence of the wall in this system. When the granular assembly drops, during the compaction the particle contacts are being compressed. During the tapping, this compression is released: For the dry system (gray curve), the particle packing seems to allow only upward reconfiguration, while for the system with fluid (black curve), lubrication viscosity seems to compete in such a way that there is hardly any change (Figure 11).

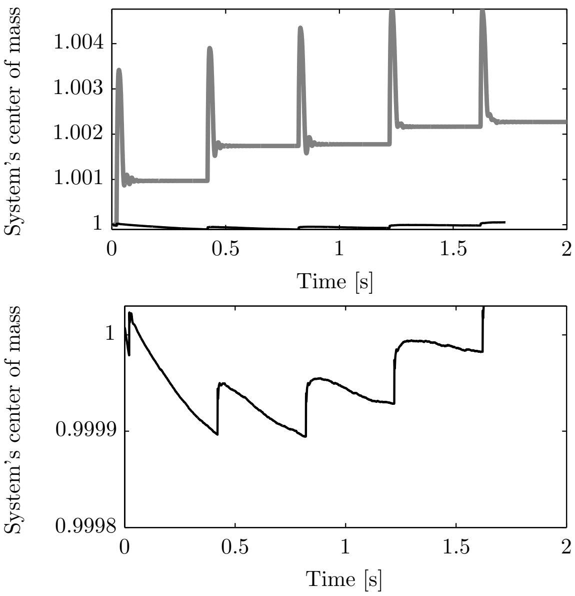

FIGURE 11. Compaction of the narrow system for the dry (above, solid line in gray) and the immersed particles (above, solid line in black), as well as latter zoomed (below).

8. CONCLUSION AND SUMMARY

Our simulation has shown that the addition of fluid to a granular assembly can increase the sound velocity in the system, compared to the dry case. The introduction of fluid into the slow dynamics of compaction of granular particles via tapping even for our single parameter with only one value for the density and viscosity showed a considerable variation of effects. For a wide system, the high viscosity slowed down the compaction, irrespective whether the system was tapped only on the ground or on the whole boundary. For a narrower, but higher system with about the same number of particles, the dynamics was altered considerably reversed: While for the dry system, the center of mass was rising, over the timescale considered, there was no motion for the system immersed in fluid.

REFERENCES

1. J. B. Knight, C. G. Fandrich, C. N. Lau, H. M. Jaeger, and S. R. Nagel, *Physical Review E* **51**, 3957–3963 (1995).
2. E. Ben-Naim, J. Knight, E. Nowak, H. Jaeger, and S. Nagel, *Physica D: Nonlinear Phenomena* **123**, 380–385 (1998).
3. E. R. Nowak, J. B. Knight, M. L. Povinelli, H. M. Jaeger, and S. R. Nagel, *Powder Technology* **94**, 79–83 (1997).
4. P. Philippe, and D. Bideau, *Physical Review E* **63**, 051304 (2001).
5. P. Philippe, and D. Bideau, *EPL (Europhysics Letters)* **60**, 677 (2002).
6. P. Philippe, and D. Bideau, *Physical Review Letters* **91**, 104302 (2003).
7. Ph. Ribière, P. Richard, P. Philippe, D. Bideau, and R. Delannay, *The European Physical Journal E* **22**, 249–253 (2007).
8. J. A. Dijksman, and M. van Hecke, *EPL (Europhysics Letters)* **88**, 44001 (2009).
9. G. Lumay, and N. Vandewalle, *Physical Review E* **70**, 051314 (2004).
10. E. Caglioti, V. Loreto, H. J. Herrmann, and M. Nicodemi, *Physical Review Letters* **79**, 1575–1578 (1997).
11. J.-M. Hertzsch, *The European Physical Journal B - Condensed Matter and Complex Systems* **18**, 459–466 (2000).
12. V. Ratnaswamy, A. Rosato, D. Blackmore, X. Tricoche, N. Ching, and L. Zuo, *Granular Matter* **14**, 163–168 (2012).
13. T. Boutreux, and P. G. de Gennes, *J. Phys. I France* **6**, 1295–1304 (1996).
14. T. Akiyama, priv. comm. (2001).
15. Y. Pan, T. Tanaka, and Y. Tsuji, *Physics of Fluids* **13**, 2320–2337 (2001).
16. S. A. M. E. Shourbagy, S. Okeda, and H.-G. Matuttis, *Journal of the Physical Society of Japan* **77**, 034606 (2008).
17. H.-G. Matuttis, *Granular Matter* **1**, 83–91 (1998).
18. P. A. Cundall, and O. D. L. Strack, *Géotechnique* **29**, 47–65 (1979).
19. H.-G. Matuttis, and A. Schinner, *International Journal of Modern Physics C* **12**, 1011–1021 (2001).
20. M. P. Allen, and D. J. Tildesley, *Computer Simulation of Liquids*, Oxford Science Publications, Clarendon Press, 1996.
21. P. M. Gresho, R. L. Sani, and M. S. Engelman, *Incompressible flow and the finite element method: isothermal laminar flow*, vol. 2, John Wiley and Sons, 2000.
22. S. H. Ng, and H.-G. Matuttis, *Theoretical and Applied Mechanics Japan* **60**, 105–115 (2012).
23. S. H. Ng, and H.-G. Matuttis, *Theoretical and Applied Mechanics Japan* **59**, 323–333 (2011).
24. K. L. Johnson, *Contact Mechanics*, Cambridge University Press, 1987.